Astron. Astrophys. 359, 433–446 (2000)

ASTRONOMY AND ASTROPHYSICS

Extraplanar diffuse ionized gas in a small sample of nearby edge-on galaxies⋆

J. Rossa and R.-J. Dettmar

Astronomisches Institut der Ruhr-Universität Bochum, 44780 Bochum, Germany

Received 21 October 1999 / Accepted 20 April 2000

Abstract. We present narrowband Hα imaging data of a small survey of nearby edge-on spiral galaxies, aiming at the detection of 'extraplanar' diffuse ionized gas (DIG). A few of our studied edge–on spirals show signs of disk–halo interaction (DHI), where extended line emission far above the galactic plane of these galaxies is detected. In some cases an extraplanar diffuse ionized gas (eDIG) layer is discovered, e.g., NGC4634, NGC 3044, while other galaxies show only filamentary features reaching into the halo (e.g., IC 2531) and some galaxies show no sign of eDIG at all. The extraplanar distances of the DIG layer in our narrowband Hα images reach values of $z \leq$ 2 kpc above the galactic plane. The derived star formation rates ($SFRs$) from the Hα flux of the studied galaxies range from $0.05 - 0.7\,\mathrm{M}_\odot\,\mathrm{yr}^{-1}$, neglecting a correction for internal absorption. The variation of the SFR values among our sample galaxies reflects the diversity of star formation within this sample. A diagnostic diagram is introduced, which allows to predict the existence of gas halos in 'quiescent' galaxies based on the ratio $\mathrm{S}_{60}/\mathrm{S}_{100}$ versus $L_{\mathrm{FIR}}/D_{25}^2$ in this diagram. We compare the positions of the non–starburst galaxies with starburst galaxies, since these galaxies populate distinct positions in these diagrams.

Key words: galaxies: halos – galaxies: spiral – galaxies: starburst – galaxies: ISM – galaxies: structure

1. Introduction

In recent years diffuse ionized gas (DIG) frequently also called warm ionized medium (WIM) has been identified as an important component of the ISM, in particular with regard to the influence of SF on the large scale distribution and physical properties of the ISM. This gas component typically has a very low electron density of $< /n/ > \sim 0.08\,\mathrm{cm}^{-3}$ (in the disk) which decreases exponentially towards the halo and is characterized through a temperature of $T = 8000$–10000 K. For a detailed review on recent developments concerning the disk–halo connection, which is briefly described below, we refer to Dettmar (1995) or Dahlem (1997).

In our own galaxy DIG was first detected as an extraplanar gas layer (Hoyle & Ellis 1963) by radio observations. In the early seventies Hα observations were performed which also showed an extraplanar layer, (see e.g., Reynolds 1984) which is now known as the 'Reynolds layer'. Only as recently as 1990 this gas component has been detected in external galaxies outside traditional H II regions (Dettmar 1990; Rand et al. 1990)

Since the DIG is traced by Hα emission, several studies have been dedicated to detect eDIG in external galaxies with the use of narrowband Hα CCD imaging, preferentially in edge–on galaxies, where the halo separates from the disk (e.g., Pildis et al. 1994; Rand et al. 1992; Rand 1996; this work). About two dozen galaxies have been detected up to now that show signs of disk–halo interaction (DHI). Subsequent longslit spectroscopy has been performed for a few galaxies including NGC 891 (Dettmar & Schulz 1992; Keppel et al. 1991; Rand 1997; Rand 1998), NGC 4631 (Golla et al. 1996), NGC 2188 (Domgörgen & Dettmar 1997), NGC 1963 & NGC 3044 (Tüllmann & Dettmar 2000), among a few others. DIG detections in starburst galaxies seem to be a common feature, as it was evidenced by an investigation by Lehnert & Heckman (1995). DIG typically reaches scale–heights in edge–on galaxies of ∼1–2 kpc, but as in the case of NGC 891 spectroscopic investigations have shown that DIG even can be detected at extraplanar distances of up to 5 kpc (Rand 1997).

The most likely process for ionizing the DIG is photoionization (Mathis 1986; Domgörgen & Mathis 1994). Although photoionization by OB stars (e.g., Miller & Cox 1993; Dove & Shull 1994) is regarded as the primary process, other mechanisms have been invoked such as shock-ionization (Chevalier & Clegg 1985), and turbulent mixing layers (Slavin et al. 1993) to account for the observed emission line ratios.

A mechanism for the transport of gas and radiation into the halo has been formulated in the late eighties (Norman & Ikeuchi 1989). The gas emanates from star forming regions in the disk of the galaxies into the halo via so called *chimneys*. This is a modified theoretical description of the formerly developed theory of galactic fountains (Shapiro & Field 1976). In the chimney scenario gas is driven by collective supernovae. Starburst driven

Send offprint requests to: jrossa@astro.ruhr-uni-bochum.de

⋆ Based on observations collected at the European Southern Observatory, La Silla, Chile

Table 1. Journal of observations

Galaxy	Date	Instrument	Hα filter λ_c [Å]	FWHM [Å]	Hα exposures	R-band exposures	Seeing
NGC 1963	20/02/1993	EFOSC II	6571.86	61.22	2×1800 sec	900 sec	$1\farcs2$
IC 2531	08/05/1991	EMMI	6607.14	71.32	1×1800 sec	600 sec	$1\farcs2$
IC 2531	21/02/1993	EFOSC II	6651.69	61.30	2×1800 sec	900 sec	$1\farcs4$
NGC 3044	20/02/1993	EFOSC II	6571.86	61.22	2×1800 sec	900 sec	$1\farcs1$
NGC 4302	21/02/1993	EFOSC II	6571.86	61.22	2×1800 sec	900 sec	$1\farcs0$
NGC 4402	20/02/1993	EFOSC II	6571.86	61.22	2×1800 sec	900 sec	$1\farcs1$
NGC 4634	20/02/1993	EFOSC II	6571.86	61.22	2×1800 sec	900 sec	$1\farcs1$
NGC 5170	07/05/1991	EMMI	6607.14	71.32	1×1800 sec	600 sec	$0\farcs8$
IC 4351	08/05/1991	EMMI	6607.14	71.32	2×1800 sec	600 sec	$1\farcs0$
UGC 10288	08/05/1991	EMMI	6607.14	71.32	2×1800 sec	600 sec	$0\farcs9$

winds that cause outflows may also play an important role, at least in nuclear starburst galaxies (Heckman et al. 1990).

A larger sample of starburst galaxies has been studied by Lehnert & Heckman (1995). Since the DIG is generally believed to be correlated with the star formation activity in the underlying galaxy disk, in starburst galaxies DIG is detected relatively frequently, and seems to be a common feature, wherby in normal galaxies not all show any disk–halo interaction. A minimum energy input to the ISM is obviously necessary in order to show any outflow phenomena. Therefore there is the demand to study more edge–on galaxies in order to make quantitative statements. This first mini–survey, which we present in the following chapters, is the first part of a larger and much more quantitative survey which is currently under investigation (Rossa & Dettmar, in prep.)

While it is spectroscopically possible to obtain physical parameters using diagnostic line ratios (Osterbrock 1989), narrowband imaging can be used to investigate the morphology of the eDIG in detail and allows correlations with other wavelength bands such as radio continuum and X–rays.

In the case of NGC 891 a 'thick disk' has been discovered by radio continuum observations, that show a correlation with the eDIG in Hα (Dahlem et al. 1994). Also some X–ray observations show a correlation, wherby here the hot ionized gas (HIM) is traced. The X–ray halo emission is a result of the interaction between the gas flows of supernovae explosions and/or star winds that are expelled from the starforming regions in the disk, which interact with the surrounding medium in the halo. These observations have aimed at the spatial extend which can be compared with the eDIG in optical observations. (e.g., Bregman & Pildis 1994; Fabbiano et al. 1990; Dahlem et al. 1998). Moreover the dust features seen in several edge–on galaxies at high galactic latitudes with typically $z \sim$ 300–1000 pc (e.g., Howk & Savage 1997, 1999; Rossa & Dettmar, in prep.) can also be compared with the DIG distribution.

2. Observations and data reduction

2.1. Hα imaging

The basis of our Hα survey consist of 9 galaxies, for which data have been obtained in two observing runs with two different instruments. Optical Hα narrow–band images of 6 edge–on spiral galaxies have been obtained with the ESO Faint Object Spectrograph Camera 2 (EFOSC2) in imaging mode, attached to the ESO/MPI 2.2m telescope at La Silla, Chile on Feb. 20–21 1993. The used CCD was the ESO CCD#19 TH–chip with a pixel array of 1024×1024 pixel. The pixel scale is $0\farcs34\,\mathrm{pix}^{-1}$. The narrowband images were taken through the ESO Hα filters No. 694, 697, and 439. The equivalent widths of the filters are 32.4, 32.6, 44.3Å respectively. The total integration times of the Hα images were 3600 sec. on average, splitted into two images. The journal of the observations is given in Table 1. Additional R–band images have been obtained in order to perform a continuum subtraction. The integration times were 10–15 minutes for each galaxy in the R–band.

In addition a small sample consisting of 4 edge–on spirals have been observed with the ESO Multi Mode Instrument (EMMI) at the NTT in imaging mode. The observations have been carried out during May 7–8 1991. In this observing campaign the ESO CCD–chip #24 has been used. The FA–2048–L chip has a pixel array of 2048×2048 pixel. The achieved pixel scale is $0\farcs27\,\mathrm{pix}^{-1}$. The H$\alpha$ images were all taken through the ESO filter No. 595. For the Hα images the integration times were 1800 sec and 3600 sec. The R–band integration times were 600 sec each (see Table 1). Since the edge–on spiral IC 2531 has been observed in both observing runs, 9 galaxies in total have been investigated.

2.2. Data reduction

The data reduction was performed in the usual manner using the IRAF[1] packages, including bias level correction, flat–fielding in order to remove the sensitivity variations. The images have been background corrected. This was done by measuring the intensity of various regions in the CCD image field that were neither contaminated by galaxy emission nor by bright stars, that contribute to a certain level to the background intensity. The field size of the boxes chosen for the background subtraction was typically ∼50 pix×30 pix. Usually three different fields were

[1] IRAF is distributed by the National Optical Astronomy Observatories, which is operated by the Association of Universities for Research in Astronomy, Inc. (AURA) under cooperative agreement with the National Science Foundation.

measured, to get a median level for the background, which was subtracted for each galaxy frame.

In order to study the Hα emission in the galaxies, the continuum emission in the filter passband has to be corrected. For this purpose the R–band images had to be scaled and subtracted from the Hα images. This was done in the following way. First the R–band and Hα line images had to be aligned. For that purpose the pixel coordinates of three to four stars in each frame have been measured and the Hα frames have finally been shifted accordingly. Then the countrates of a region in the galaxy which was considered free from Hα emission have been determined in both the R and Hα images. The ratio of the two determined values is the scaling factor. The R-band image was divided by that value and then subtracted from the Hα image. By that procedure a continuum free Hα+[N II] image is created. Finally the two Hα images have been combined to gain a better S/N ratio. Some cosmics have been removed manually. The detection of cosmics was straight forward since we had two Hα images for each galaxy, which can be easily compared.

Finally a flux calibration has been performed. The measured R–band photometry data of our edge–on galaxies have been taken from NED[2]. These R–band magnitudes represent measured magnitudes in a certain aperture. Therefore we determined the flux (countrates) in our R–band image for the same aperture size as were the photometry data, applying the flux of the standard Vega as a calibrator. We then divided the calculated flux by the value of the measured countrates in our R–band filter, correcting for the integration time and the scaling factor of our passband exposures. Finally we multiplied this factor with the measured countrate in our Hα exposure and thus get the relation between the countrates and the flux. The uncertainties with this method are of the order of 20%.

3. Analysis

With the transformed flux units it is also possible to convert the flux values to another commonly used unit, namely the emission measure (EM) which is defined by

$$EM = \int_0^r n_\mathrm{e}^2 \, dl \tag{1}$$

The emission measure can be calculated according to

$$EM = 2.75 \times T_4^{0.9} \, I(\mathrm{H}\alpha) \, \mathrm{cm}^{-6} \, \mathrm{pc} \tag{2}$$

with I(Hα) the intensity of the Hα emission, in Rayleigh (R), and with T the gas temperature in units of 10^4 K. (Reynolds 1990), assuming case B photionisation (Osterbrock 1989). Usually a conversion is derived at Hα where $1\,\mathrm{cm}^{-6}\,\mathrm{pc} = 2.06 \times 10^{-18} \mathrm{erg\,s^{-1}\,cm^{-2}\,arcsec^{-2}}$.

Although the continuum has been subtracted from the images, there is still some contamination of the Hα line from the nearby [N II] doublet, which also contributes to the line emission. This is due to the given filter passband. With knowledge of line ratios, derived from spectroscopical investigations, the mean ratio of Hα to [N II] can in principle be determined, which in turn can be used to correct for the [N II] emission. From the measured Hα line flux the total Hα luminosity can be computed by

$$L_{\mathrm{H}\alpha} = 4\,\pi\,D^2\,F_{\mathrm{H}\alpha} \tag{3}$$

where D is the distance to the galaxy. It is now possible to derive the star formation rate (SFR) using the calibration of Madau et al. (1998) to a Salpeter initial mass function (IMF) with mass limits 0.1 and 100 $\mathrm{M}_\odot$ (Salpeter 1955) which after Kennicutt (1998b) yields

$$SFR\,[\mathrm{M}_\odot\,\mathrm{yr}^{-1}] = 7.9 \times 10^{-42}\,L_{\mathrm{H}\alpha}\,[\mathrm{erg\,s}^{-1}]. \tag{4}$$

The results can be compared with SFRs derived by far–infrared (FIR) fluxes from e.g., measurements with the IRAS satellite. The SFR, as derived from the FIR flux, are expected to be higher unless a correction of the Hα fluxes is performed for internal dust absorption (since many edge–on galaxies bear a more or less prominent dust lane). The SFR from the FIR luminosity can be calculated in a similar manner according to Kennicutt (1998b), and references therein, taking into account the timescales for bursts of SF, which yields

$$SFR\,[\mathrm{M}_\odot\,\mathrm{yr}^{-1}] = 4.5 \times 10^{-44}\,L_{\mathrm{FIR}}\,[\mathrm{erg\,s}^{-1}] \tag{5}$$

which is actually valid for starburst galaxies. The sensitivity of our observations is $7.2 \times 10^{-18}\,\mathrm{erg\,s^{-1}\,cm^{-2}\,arcsec^{-2}}$ on average, which corresponds to an emission measure (EM) of $3.5\,\mathrm{cm}^{-6}\,\mathrm{pc}$.

4. Results

4.1. The sample

Basic parameters for our sample of 9 edge–on galaxies are given in Table 2. Here the coordinates for the epoch J2000 along with morphological type, distances, heliocentric corrected radial velocities, sizes, inclinations, and R–band magnitudes are listed. The selection criteria for most of the objects of our sample were the following. Initially a list has been created from the Uppsala General Catalogue of Galaxies (UGC) (Nilson 1973) that has been used as a sample of edge–on galaxies for radio continuum observations (Hummel et al. 1991). The inclination criterium was $i \geq 75°$ in addition to the size criterium. Additional objects fulfilling the size and inclination criteria were observed to make optimal use of the Sidereal Time coverage during observations.

A further selection criterium was to study nearby galaxies. All studied objects have distances of $D \leq$40 Mpc, where the spatial resolution is sufficiently high to study morphological features (e.g., plumes) that are related to a gas outflow from the disk into the halo. We are assuming a Hubble parameter of $\mathrm{H}_0 = 75\,\mathrm{km\,s^{-1}\,Mpc^{-1}}$, that we will adopt throughout this paper. For the most distant galaxy in our sample (IC 4351) $1''$ corresponds to 172 pc, and for the nearest galaxy $1'' = 83\,\mathrm{pc}$.

[2] NASA Extragalactic Database

Table 2. Basic galaxy parameters

Galaxy[a]	R.A. (J2000)	Dec. (J2000)	Type	D [Mpc]	$v_{\rm HI}$ [km s^{-1}]	$a \times b$	i	$m_{\rm R}$[b]
NGC 1963	$05^{\rm h}33^{\rm m}12\overset{\rm s}{.}8$	$-36°23'59''$	Sc	17.7	1324	$3\overset{'}{.}8 \times 0\overset{'}{.}8$	$84\overset{\circ}{.}5$	12.11
NGC 3044	$09^{\rm h}53^{\rm m}39\overset{\rm s}{.}8$	$+01°34'46''$	SBb	17.2	1292	$5\overset{'}{.}7 \times 0\overset{'}{.}6$	$84\overset{\circ}{.}0$	11.65
IC 2531	$09^{\rm h}59^{\rm m}55\overset{\rm s}{.}7$	$-29°36'55''$	Sc	33.0	2474	$7\overset{'}{.}5 \times 0\overset{'}{.}9$	$90\overset{\circ}{.}0$	11.41
NGC 4302	$12^{\rm h}21^{\rm m}42\overset{\rm s}{.}4$	$+14°36'05''$	Sc	18.8[c]	1108[c]	$5\overset{'}{.}5 \times 1\overset{'}{.}0$	$88\overset{\circ}{.}0$	12.11
NGC 4402	$12^{\rm h}26^{\rm m}07\overset{\rm s}{.}9$	$+13°06'46''$	Sb	22.0[c]	237	$3\overset{'}{.}9 \times 1\overset{'}{.}1$	$83\overset{\circ}{.}1$	12.09
NGC 4634	$12^{\rm h}42^{\rm m}40\overset{\rm s}{.}4$	$+14°17'47''$	Sc	19.1[c]	1118[c]	$2\overset{'}{.}6 \times 0\overset{'}{.}7$	$83\overset{\circ}{.}0$	12.42
NGC 5170	$13^{\rm h}29^{\rm m}49\overset{\rm s}{.}0$	$-17°57'59''$	Sc	20.0	1503	$8\overset{'}{.}3 \times 1\overset{'}{.}0$	$83\overset{\circ}{.}1$	10.77
IC 4351	$13^{\rm h}57^{\rm m}54\overset{\rm s}{.}1$	$-29°18'54''$	Sb	35.5	2662	$5\overset{'}{.}8 \times 1\overset{'}{.}1$	$78\overset{\circ}{.}9$	11.18
UGC 10288	$16^{\rm h}14^{\rm m}25\overset{\rm s}{.}1$	$-00°12'27''$	Sc	27.3	2045	$4\overset{'}{.}7 \times 0\overset{'}{.}5$	$83\overset{\circ}{.}4$	12.20

[a] All data have been taken or were calculated from the RC3 (de Vaucouleurs et al. 1991), except where indicated
[b] taken from NED, and from Schroeder & Visvanathan 1996
[c] taken from Teerikorpi et al. 1992

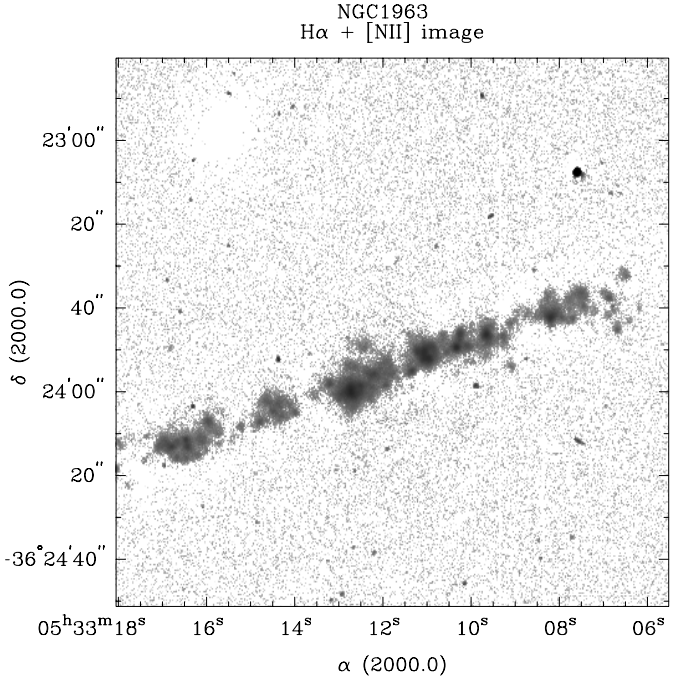

Fig. 1. Hα+[N II] image of NGC 1963. The scale is $1'' = 86\,{\rm pc}$

All 9 galaxies of our sample are late–type galaxies (Sb–Sc), and DIG has been detected in galaxies of this type before, as already mentioned in Sect. 1. Five of them show an eDIG layer with extraplanar distances of $z \leq 2$ kpc above the galactic midplane, whereby 1 galaxy shows only plumes or filaments reaching into the halo. In Table 4 we give a summary of the observed DIG features, that will be reviewed in detail for each galaxy below.

4.2. Individual results for each galaxy

In this section we present the results for each of our selected galaxies separately and discuss them in Sect. 5. The field sizes of the figures have been chosen conveniently to show the larger galaxies entirely, except for IC 2531 which did not fit completely in the field of view. The smaller ones are shown as enlargements to give more details. Spatial profiles of the DIG emission are presented in Fig. 8.

NGC 1963

This galaxy has been classified as type Sc (Lauberts 1982). NGC 1963 is poorly studied. It appears in the extended 12 micron galaxy sample (Rush et al. 1993) with measured fluxes of $F_{60\mu{\rm m}}$ = 2.99 Jy and $F_{100\mu{\rm m}}$ = 7.38 Jy. An elliptical galaxy is visible $\sim 1\overset{'}{.}5$ to the NNE. This is a member of the galaxy cluster Abell S0535, which is at a distance of z = 0.0473 (Quintana & Ramírez 1995) and hence not associated with NGC 1963. It is important to check the surrounding field of a galaxy for companion galaxies, as those galaxies – if closeby to the parent galaxy (e.g., same redshift) – may also trigger gas outflows. Due to the scaling procedure this elliptical galaxy is not visible in the Hα image (it looks like an outmasked image) as objects with no or almost non–detectable Hα emission appear. (The two white vertical lines are dead–pixel columns).

A weak eDIG layer is seen (0.5–0.6 kpc on average) as well as several extraplanar patches on either side of the galaxy disk. The most prominent feature is just north of the center (R=0.2 kpc). It is located at $z \approx 0.7\,{\rm kpc}$ above the galactic plane. The extended emission is seen around several bright H II regions, that are not continuously distributed along the galaxy plane. They are more or less clustered in small groups. The Hα flux of the galaxy is estimated to be $1.64 \times 10^{-13}\,{\rm erg\,s^{-1}\,cm^{-2}}$ and from the derived Hα luminosity the global star formation rate (SFR) has been determined which is $SFR = 0.05\,{\rm M_\odot\,yr^{-1}}$.

The stars in the Hα images usually appear as residuals due to the slightly different point spread function in the various filters. The resulting Hα image is shown in Fig. 1.

NGC 3044

There has been a slight controversy, whether this galaxy is a galaxy with enhanced star formation (SF), hence with higher

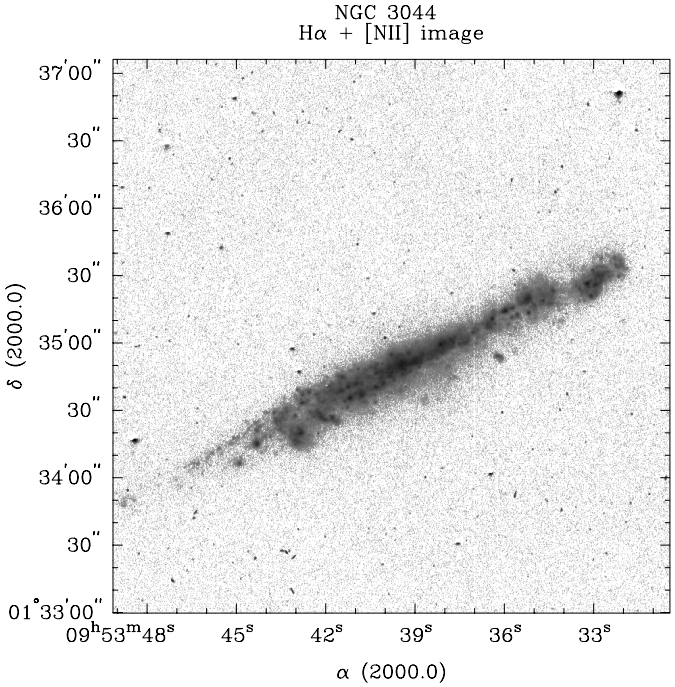

Fig. 2. Hα+[N II] image of NGC 3044. $1''$ corresponds to 83 pc

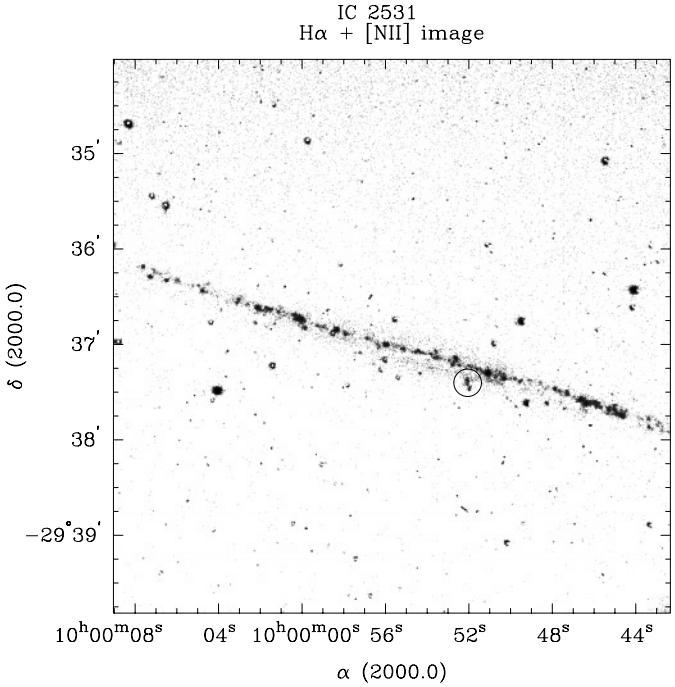

Fig. 3. Hα+[N II] image of IC 2531. The image measures $5\farcm8 \times 5\farcm8$, which is the field of view of EFOSC II in the used configuration. Therefore the galaxy disk is not covered entirely. $1'' = 160\,\mathrm{pc}$

SF than in 'normal' (quiescent) galaxies, or whether it is a starburst galaxy. In a recent survey of DIG emission in edge–on starburst galaxies (Lehnert & Heckman 1995) NGC 3044 has also been included, while other researchers classify it as a non–starburst galaxy (Hummel & van der Hulst 1989; Dahlem et al. 1995). However, the galaxy has been listed in the sample of IRAS bright galaxies (Soifer et al. 1987), so there seems clear evidence for enhanced SF but it is presently not clear if NGC 3044 hosts a starburst nucleus. In a spectroscopic study where the DIG was investigated at two different slit positions perpendicular to the galaxy disk, the positions of the detected DIG in the diagnostic diagrams fall in between the areas occupied by normal H II regions and starburst (Tüllmann & Dettmar 2000). Therefore no clear answer of this debate can be given yet. Even the term 'starburst' is sometimes not clearly defined, as various researchers use different definitions. We will come back to this point in Sect. 5.

The galaxy type is listed as SBc (Tully 1988). Even classifications as a non–barred galaxy (Sc) are listed (Nilson 1973). There are indications that in NGC 3044 a bar is present, and H I kinematics by Lee & Irwin (1997) has indeed discerned a bar. It might be worth to notice that in the eighties a supernova (SN1983E) has been detected in this galaxy (Barbon et al. 1989).

In Fig. 2 we present the Hα image. The morphology of the DIG shows various features. An eDIG layer can be detected at extraplanar distances up to $z = 0.8 - 1\,\mathrm{kpc}$. Several single plumes can also be discerned. South of the galactic plane an extended structure is visible, which has a loop–like appearance. This loop extends out to ~ 1.8 kpc with a radius of about 1 kpc, and resembles the galactic supershells. The disk appears slightly warped, which is also apparent in the R–band image. The Hα flux of the galaxy has been estimated to be $2.50 \times 10^{-12}\,\mathrm{erg\,s^{-1}\,cm^{-2}}$ and from the computed Hα luminosity the (global) star formation rate (SFR) has been derived, which is $\mathrm{SFR} = 0.71\,\mathrm{M_\odot\,yr^{-1}}$.

IC 2531

This southern edge–on spiral is slightly larger than the EFOSC2 field of view which is $5\farcm8 \times 5\farcm8$. IC 2531 is seen perfectly edge–on. In our Hα image almost no extraplanar diffuse emission has been detected. One filament (the chimney–like feature) is clearly seen, emerging from the disk radius at R=6 kpc south of the plane into the halo (see Fig. 3). This feature is marked in Fig. 3 with a circle. It reaches a height of z=2 kpc above the galactic plane. The Hα image looks pretty much like a string of pearls. Several disk H II regions can be identified, but only the largest are surrounded by DIG, which is probably not extraplanar. Only at R=8.4 kpc from the center a larger disk H II region seems to be embedded in a fainter DIG layer reaching an extraplanar height of z=1.1 kpc.

There are no radio continuum observations available, and the only conspicous feature seen in the R-band images is a 'peanut-bulge'. IC 2531 looks similar to the well studied edge–on spiral NGC 891 in the optical. However, in Hα they appear totally different. No Far–Infrared (FIR) emission has been detected with the IRAS satellite in IC 2531. Therefore it can be concluded, that the SFR in this edge–on spiral is completely different from that in NGC 891. From a theoretical study in comparison with multi–color surface brightness profiles, observations to model the vertical structure of the disk it is found that the disk

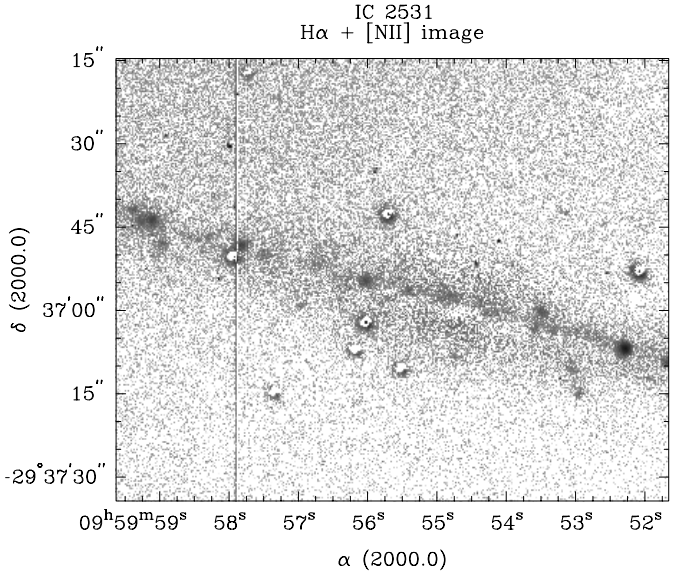

Fig. 4. Central part of the Hα+[N II] image of IC 2531, obtained with the NTT

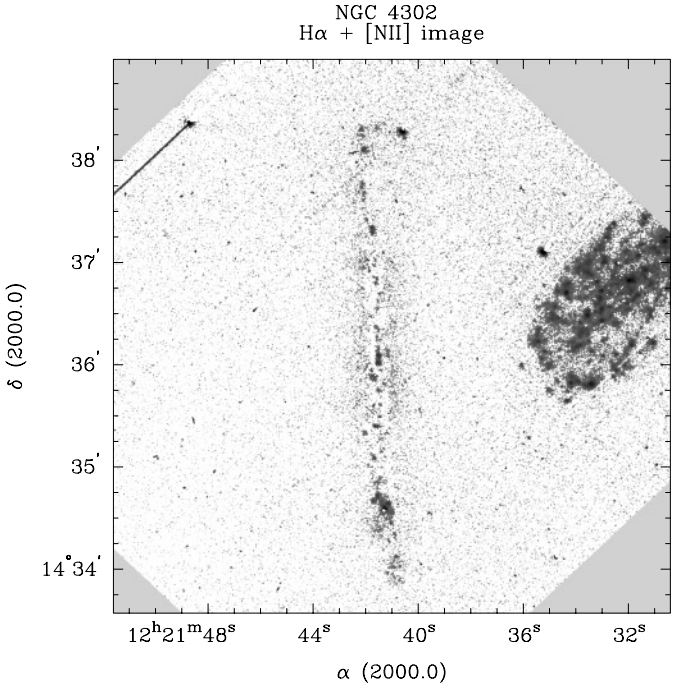

Fig. 5. Hα+[N II] image of NGC 4302. The face–on spiral on top right is NGC 4298. $1'' = 91$ pc

in IC 2531 has a similar composition as the disk of our Milky Way (Just et al. 1996).

In Fig. 4 we show an enlargement of the central part of IC 2531. This image has been obtained with the NTT. Here the filament south of the galaxy disk can be seen in a little more detail. The proof that this filament is real and not an artifact is given by its presence in both of our images, taken with different instruments. Furthermore we have always obtained two exposures for each galaxy with any given instrumental setup, where we can distinguish between faint emission and cosmics that sometimes can mimic faint emission. Since DIG is traced by Hα emission, it is evident that there is low SF activity in the disk of IC 2531.

NGC 4302

This edge–on galaxy has already been studied before in the DIG context with Hα imaging by two different groups (Pildis et al. 1994; Rand 1996). In our Hα we see faint eDIG emission, when averaging the intensities perpendicular to the galaxy disk. This is consistent with the results from Rand (1996), who also detected eDIG. The single plume, already detected by Pildis et al. (1994), is also visible in our image. The halo emission in NGC 4302 is fainter than in NGC 3044. However, the halo emission is much brighter than the emission from the disk. This is due to the extended dust lane (which is very prominent in NGC 4302) along the disk. The dustlane absorbs most of the disk emission. Most of the other galaxies in our sample are not as much influenced by thick dust lanes as it is the case in NGC 4302. The dust lanes are best visible in broadband images. In our Hα image NGC 4302 (see Fig. 5) is shown with a companion galaxy, the face–on spiral NGC 4298. Whether this galaxy is capable to trigger the star formation in NGC 4302 is not known yet.

NGC 4402

In this edge–on spiral an eDIG is detected showing extraplanar distances of ~ 2.2 kpc. The DIG emission is restricted to the eastern part of the galaxy. Small filaments are emanating the galaxy north of the galactic plane. Parts of the spiral structure can be discerned in the Hα image due to the deviation from the exact edge–on sightline of $\Delta i \sim 7°$. NGC 4402 is a member of the Virgo cluster (cf. Binggeli et al. 1985). Dozens of relatively bright H II regions are embedded in DIG. This DIG is supposed to originate from emission that is leaking through the H II regions heated by hot O and B stars. The Hα image is shown in Fig. 6. The visual appearance of NGC 4402 is similar to the recently studied Virgo cluster member galaxy NGC 4522 (Kenney & Koopmann 1999). They claim that they have detected eDIG up to 3 kpc above the galactic plane. However, the inclination of that galaxy is far away from being edge–on, so the observed emission might be emission from the disk.

The Hα flux of NGC 4402 has been estimated and has a value of $1.47 \times 10^{-13}\,\mathrm{erg\,s^{-1}\,cm^{-2}}$ and from the derived Hα luminosity the star formation rate (SFR) has been determined which is $SFR = 0.07\,\mathrm{M_\odot\,yr^{-1}}$.

NGC 4634

This edge–on galaxy is also a member of the Virgo cluster (cf. Binggeli et al. 1985; Helou et al. 1984) and Teerikorpi et al. (1992) give a distance of 19.1 Mpc to this galaxy. Recently new R–band photometry became available for this galaxy and other members of the Virgo Cluster (Schroeder & Visvanathan 1996). Oosterloo & Shostak (1993) list it as a binary pair with

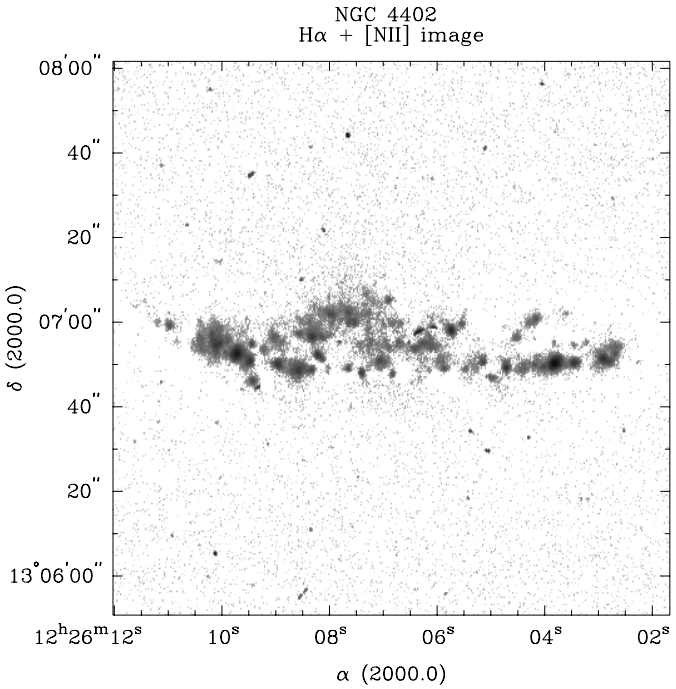

Fig. 6. Hα+[N II] image of NGC 4402. The scale is $1'' = 107\,\mathrm{pc}$

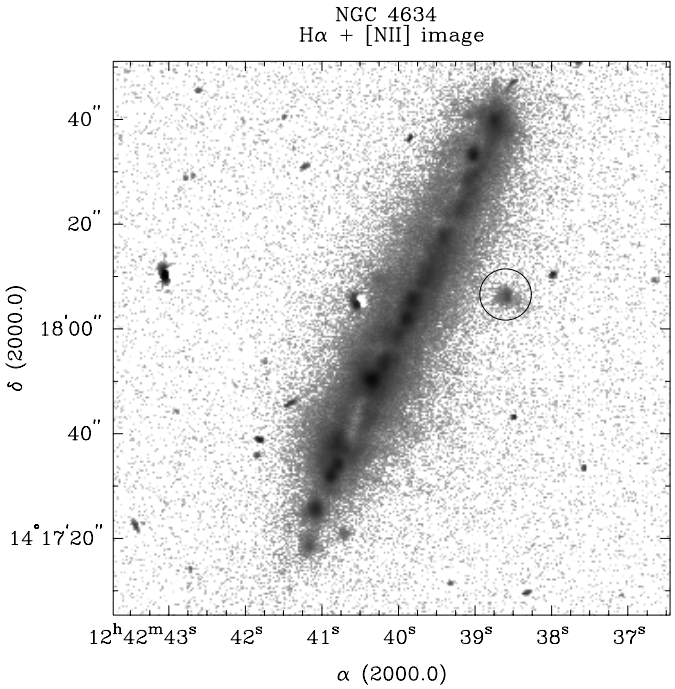

Fig. 7. Hα+[N II] image of NGC 4634. A bright eDIG layer is clearly visible. The extraplanar emission region (Patch 1) is marked by a circle. The scale is $1'' = 93\,\mathrm{pc}$

NGC 4633 in their H I study. NGC 4634 shows an interesting DIG morphology. A bright eDIG layer is detected, which reaches distances of $\sim$1.1 kpc above the galactic plane. We show our Hα+[N II] image in Fig. 7. In addition to the eDIG layer, several filaments reach into the halo, similar to the ones discovered in the edge–on spiral NGC 5775 (Dettmar 1993). These plumes are more frequent than in NGC 5775, although fainter in intensity on average.

Furthermore several H II regions in the disk can be identified, and in the south–eastern part a possible dust region absorbs parts of the emission from the disk. Interestingly the visible H II regions in the disk seem not aligned in a plane. This might be an orientation effect due to the galaxy inclination of $83°$. However, the position of the H II regions along the plane scatter randomly, which might indicate that the disk is disturbed. Therefore an interaction of NGC 4634 with neighbouring galaxies in the Virgo cluster seems likely.

In the vicinity of NGC 4634 another Virgo spiral is located, namely NGC 4633. Both galaxies have similar radial velocities ($\Delta \mathrm{v} \approx 112\,\mathrm{km\,s^{-1}}$), therefore a direct interaction seems very likely. The presence of a bar is reported in the literature, which could also be a source of disturbance.

About 10 bright H II regions can be identified in the disk which are embedded in DIG. Some of the filaments reaching into the halo, which are seen in our Hα image, can be traced back to the disk. This would be consistent with theoretical models ('chimneys'), with the chimneys as the interface between disk and halo. At least one H II region protudes from the disk. This is the second bright emission region in the very northern part of the disk, which is slightly offset from the disk.

The most outstanding feature is seen NW of the galaxy disk in the halo. This feature, which we refer to as Patch 1, is a small isolated emission patch, that is clearly visible in our Hα images, located $\sim$1.4 kpc above the galactic plane. Whether this prominent feature is related to the eDIG is not clear yet. Additional longslit spectroscopy is necessary to reveal the true nature of this object, whether it is truly related to the eDIG or rather a (projected) dwarf galaxy. However, if this morphological feature, which seems to show no direct connection (at the faint level) to the disk, will indeed be confirmed spectroscopically (e.g., same redshift) as part of the eDIG in NGC 4634, this would give rise to a new phenomenon visible in halos of edge–on galaxies which might be coined as *star formation in galactic halos*. No object was found in a search of the NED and SIMBAD databases at this position.

In Fig. 8 we present cuts perpendicular to the major axis of our studied edge–on galaxies. Typically 30 pixel scans have been averaged along the minor axis. In these spatial profiles the Hα flux in $\mathrm{erg\,s^{-1}\,cm^{-2}}$ is plotted as a function of the spatial coordinate (z). For NGC 4634 the highest peak corresponds to the disk and halo region and the secondary peak to the right is the emission patch Patch 1, located about 1.4 kpc above the galactic plane. The Hα flux of NGC 4634 has been estimated, without correcting for internal absorption, to be $1.47 \times 10^{-12}\,\mathrm{erg\,s^{-1}\,cm^{-2}}$ and from the computed Hα luminosity the SFR has been derived ($SFR = 0.51\,\mathrm{M_\odot\,yr^{-1}}$).

A radio continuum flux (flux density) at λ = 2.8 cm of 6 $\pm$1 mJy and at λ = 6.3 cm of 20 $\pm$2 mJy has been reported (Niklas et al. 1995) but no maps are shown, which would allow a comparison between radio continuum and Hα. No X–ray

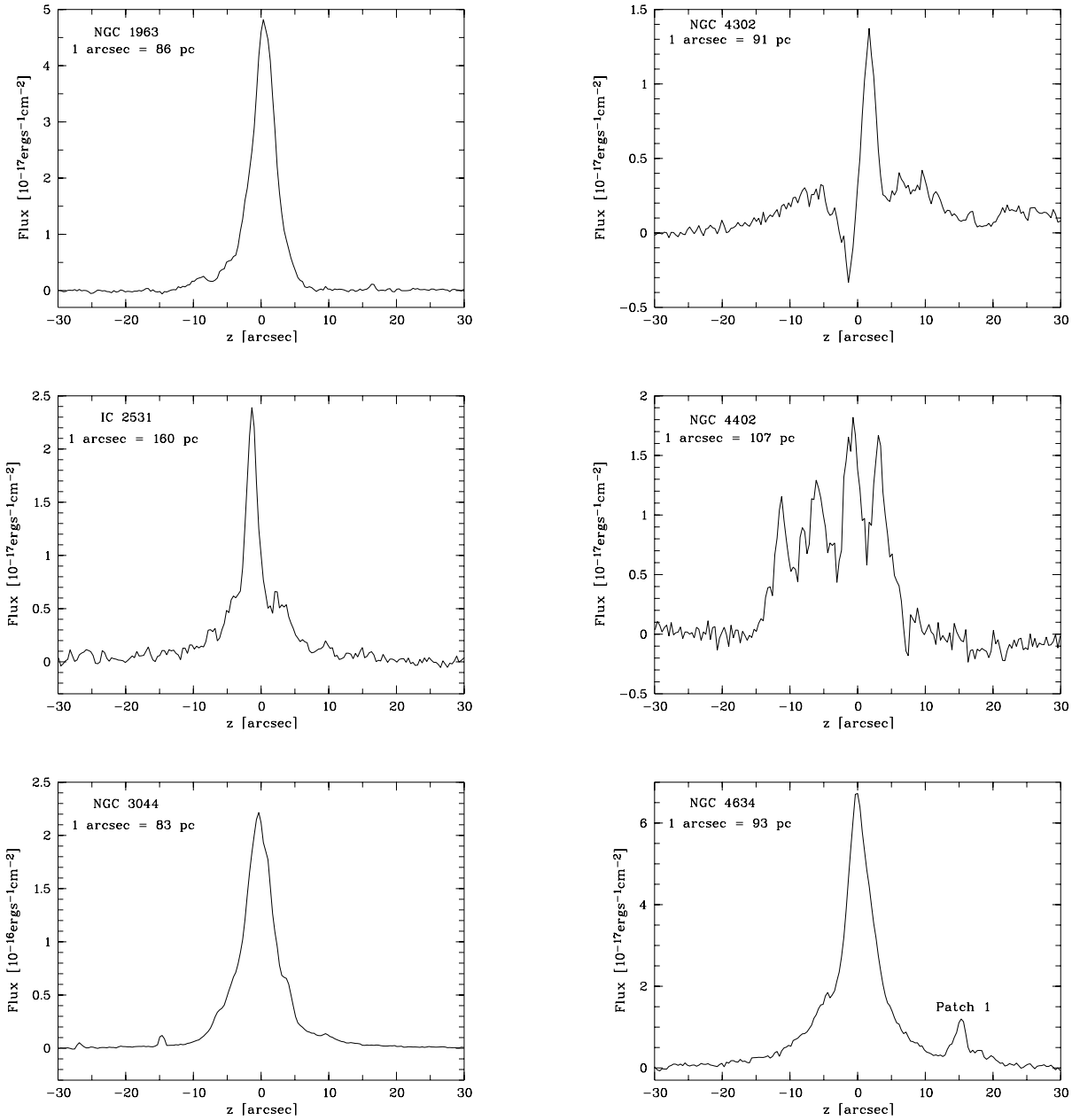

Fig. 8. Spatial profiles of the Hα emission in 6 of our studied edge–on galaxies (cuts perpendicular to the major axis). In each case several pixel rows (NGC 1963: 34, IC 2531: 22, NGC 3044: 30, NGC 4302: 78, NGC 4402: 31, and NGC 4634: 21) have been averaged around representative regions. The flux (in $\mathrm{erg\,s^{-1}\,cm^{-2}}$) is plotted as a function of the distance from the galactic plane (z) in arcseconds

observations have been performed up to now to study the hot ionized gas.

NGC 5170

This is another example of a poorly studied southern spiral galaxy. No eDIG is detected in this edge–on galaxy. Our image shows the bulge slightly oversubtracted. From the FIR flux one can expect not to have high SFRs, if one assumes a correlation between the FIR luminosity and the SFR. However, some galaxies seem to have high local SFR but not on a global scale. Therefore for an intrinsically large galaxy the integrated FIR would be lower, and a correlation with the FIR flux seems not always apropriate as a tracer for high SFR and hence for gas outflows from the disk into the halo. A better indicator for localized SF activity, which is often used, is the ratio of the FIR luminosity and the isophote diameter with 25^{th} mag/$\square''$ $[L/D_{25}^2]$ (e.g., Rand 1996). We will discuss this point in Sect. 5 in detail. The Hα image is shown in Fig. 9.

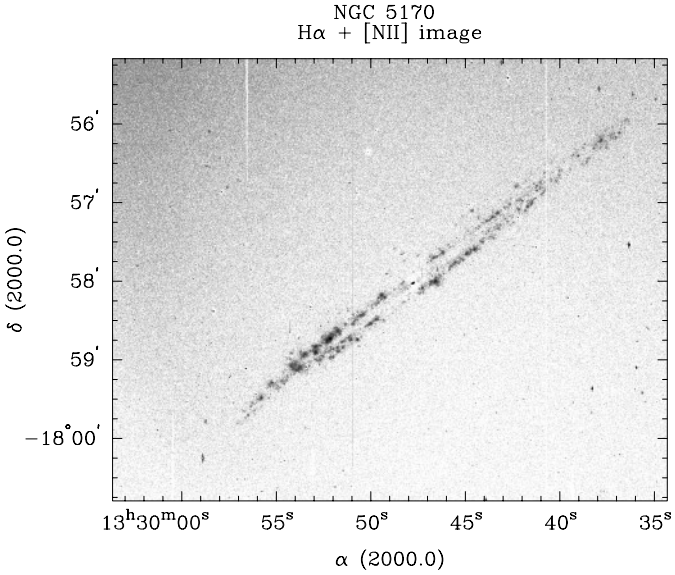

Fig. 9. Hα+[N II] image of NGC 5170. At the distance of NGC 5170, $1''$ corresponds to 97 pc

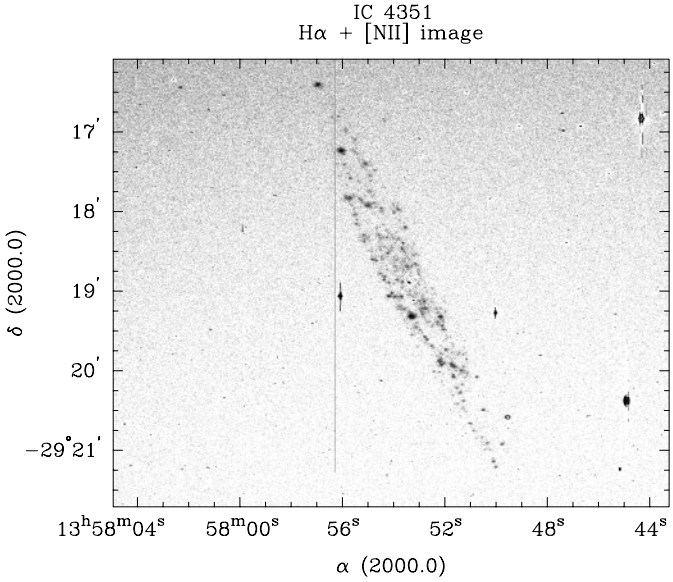

Fig. 10. Hα+[N II] image of IC 4351. At the distance of IC 4351, $1''$ corresponds to 172 pc

IC 4351

This southern edge–on spiral looks rather inconspicuous in Hα (see Fig. 10). No eDIG is detected at the sensitivity level of our data. This is the only galaxy in our sample with an inclination slighly smaller than $80°$, where the spiral pattern becomes partly visible. In starburst galaxies of similar inclination eDIG has been discovered. However, in IC 4351 no morphological features can be discerned which might be related to eDIG. This is a counter–example of a Sb galaxy in the eDIG context. This reflects that not all late–type spiral galaxies bear disk–halo interaction (DHI) at a noticable level.

UGC 10288

Already studied by Rand (1996), this galaxy has also been a target object of our survey. Unfortunately the Hα image suffers from a bad S/N ratio and thus shows only little information. Therefore it is not reproduced here. Only the brightest H II regions in the disk are visible, but no further information can be retrieved from this image.

4.3. Comparison of DIG morphology in our sample

In Table 4 we summarize the detections of the eDIG and list the morphological features for each galaxy. The morphology of the disk, as well as the halo, is presented in detail. We give the position in the (R, z) coordinates, with R the coplanar distance from the nucleus, and z the extraplanar distance. Furthermore we list references to radio continuum detections (e.g., 'thick disks') and correlations. The references of radio continuum observations are cited in Sect. 4.2 for each galaxy. Moreover we list the FIR fluxes, as measured with the IRAS satellite, and give the computed star formation rates (SFR), that have been derived from our Hα observations.

The determination of the SFRs in edge–on galaxies can generally (i.e. in the case of optical observations) only give lower limits of the true SFRs. This is basically due to internal absorption (extinction by dust), which can be quite prominent for edge–on galaxies with a strong dust lane, such as NGC 891 (Dettmar 1990). The derived SFRs in our galaxy sample are up to 10 times lower than the SFRs calculated from the FIR flux, which would be expected, since we did not apply an extinction correction. Thus our derived SFRs from the Hα flux are meant to be lower limits and for comparison between objects only.

The derived Hα luminosities of our sample galaxies with clear eDIG detections (which range from $L_{\mathrm{H}\alpha} = 6.2 \times 10^{39}\,\mathrm{erg\,s^{-1}}$ to $L_{\mathrm{H}\alpha} = 8.9 \times 10^{40}\,\mathrm{erg\,s^{-1}}$) are comparable to other spiral galaxies of the same Hubble type, which were studied for instance by Kennicutt & Kent (1983). The derived Hα flux of NGC 3044 is also in agreement with the measurement by Lehnert & Heckman (1995).

4.4. Determination of the DIG properties n_{e} and M

In the previous sections the morphology of the DIG in our studied galaxies has been discussed. We can now derive some physical quantities that are directly related to the outflowing gas. We want to address the question on which percentage of the observed DIG is actually belonging to the halo, and which fraction is related to the disk (i.e. the diffuse gas component of the H II regions in the disk). We therefore determined the Hα flux in our galaxies in various intervalls of extraplanar distances. First we determined the flux in the disk for which we assume a maximal extension of 300 pc from the galactic plane on either side of the galaxy disk. We also measured the total flux in the halo, for which we assume an extraplanar distance from 300 up to the distance of the most distant halo feature in each galaxy that is

Table 3. Fractions of DIG distributions

Galaxy	f_{halo}(Hα flux)	f_{disk}(Hα flux)	$\frac{f_{\rm halo}}{f_{\rm disk}}$
NGC 1963	$12 \pm 3\%$	$88 \pm 22\%$	0.136
NGC 3044	$41 \pm 10\%$	$59 \pm 15\%$	0.695
NGC 4302	$59 \pm 15\%$	$41 \pm 10\%$	1.439
NGC 4402	$45 \pm 11\%$	$55 \pm 14\%$	0.818
NGC 4634	$36 \pm 9\%$	$64 \pm 17\%$	0.563

visible in our images. The comparison with the total flux yielded the respective fractions, which are summarized in Table 3.

We have calculated some physical quantities which make it possible to derive the mass of the DIG. First we determined the electron density of the diffuse halo gas by combining the Eq. (1) and (2). This yields with an assumed filling factor of $f = 0.2$ (Dettmar 1992)

$$n_e = \sqrt{2.75 \frac{T_4^{0.9}}{f\,D} \frac{F_{\rm H\alpha}}{\Omega}} \tag{6}$$

With the knowledge of $n_{\rm e}$ it is now possible to give estimates of the total gas mass, which is incorporated within the halo gas. We approximate the extraplanar gas layer integrated over the galaxy disk as a cylindric geometry which gives $dV = \pi\,|z|^2\,dR$, with z as the extraplanar radius, and R as the radial extent of the galaxy. Under the assumption of $n_{\rm e} \approx n_{\rm p}$, and with $M = \int \rho\,dV$, and $\rho = n_{\rm e}\,m_{\rm p}$, this translates to

$$M_{\rm DIG} = n_{\rm e}\,m_{\rm p}\,\pi\,|z|^2\,R \tag{7}$$

The derived column densities, electron densities, and masses for our studied galaxies, which have diffuse extraplanar gas layers, are listed in Table 5 below.

For comparison we list the value of the diffuse gas mass of NGC 891, including a correction for internal extinction, that was derived by Dettmar (1990), which is $M_{\rm DIG} = 4 \times 10^8\,M_\odot$.

5. Discussion

After the first detection of eDIG in external galaxies (e.g., Dettmar 1990; Rand et al. 1990) the question was raised, whether it is a general case, that all late–type galaxies show DHI, or whether this is an exception. During the last decade a few investigations have been performed using basically optical narrowband imaging (Hα) in selected edge–on spirals. The sample sizes of these small–surveys were typically ≤ 10 galaxies. (e.g., Rand 1996; Pildis et al. 1994; Hoopes et al. 1999; this work). Additional studies in the optical regime have been carried out – mostly irregular and dwarf galaxies (e.g., Martin 1997) – and on single objects such as NGC 55 (Ferguson et al. 1996), and three Sculptor group galaxies including also NGC 55 (Hoopes et al. 1996), among a few other galaxies. In the next section we discuss our observations and compare our results with other observations, such as the Lehnert & Heckman starburst sample.

5.1. Comparison between starburst and normal (quiescent) galaxies

In an investigation by Lehnert & Heckman (1995) all IRAS bright and IRAS warm nearby edge–on starburst galaxies have been searched for extraplanar diffuse ionized gas. In this IR–selected survey 55 galaxies have been studied. This and supplementary studies have shown that all known nearby starburst galaxies show gaseous halos. These outflows most likely arise from starburst winds, driven by collective supernovae or massive star winds. This is most likely true for nuclear starbursts. However, presently it is not clear, if such a starburst wind is the driving force behind the outflows of normal or 'quiescent' galaxies. In starburst galaxies the outflows occur preferentially from the nuclear regions (nuclear or central starburst), whereas in quiescent galaxies the filaments usually do not protrude from the nuclear region, rather from the strong SF regions distributed across the disk.

The criterium for IR–bright galaxies is quoted by $S_{60} \geq 5.4$ Jy and IR–warm galaxies are denoted by $S_{60}/S_{100} \geq 0.4$ (Lehnert & Heckman 1995). Dahlem (1997) lists also a value of $S_{60} \geq 30$ Jy for IR-warm galaxies.

To illustrate differences between starburst galaxies and normal (quiescent) galaxies we have constructed diagnostic diagrams (see Fig. 11, and Fig. 12), in which the different types of galaxies populate different positions. We have plotted the ratio of the 60μm and 100μm IRAS fluxes as a function of the ratio of $L_{\rm FIR}/D_{25}^2$, which is the FIR–luminosity over the optical galaxy diameter of the $25^{\rm th}$ magnitude isophote squared. This term ($L_{\rm FIR}/D_{25}^2$) has been introduced by Rand (1996) as a tracer for star formation activity in a galaxy (star formation rate per unit area).

In Fig. 12 we have plotted the same information in logarithmic scale, in order to show more detail on the border of starburst/non-starburst galaxies. The slope gives rather empirically a division between the two object classes. In the literature some galaxies which were initially identified as a starburst galaxy later were classified as a non starburst galaxy and vice versa.

We have computed the FIR-luminosity according to

$$L_{\rm FIR} = 3.1 \times 10^{39}\,D^2\,[2.58\,S_\nu(60) + S_\nu(100)] \tag{8}$$

with S_ν (60), S_ν (100) the flux densities in Jy and with D the distance to the galaxy in Mpc. The flux densities have been taken from the catalogue of Fullmer & Lonsdale (1989). The term D_{25}^2 is expressed in kpc^2.

The sample was compiled from the starburst galaxies studied by Lehnert & Heckman (1995), the normal (quiescent) galaxies were compiled from various investigations (e.g., Pildis et al. 1994; Rand 1996; this work). In the following table (Table 6) we list some properties concerning the DIG for the non–starburst galaxies that were investigated in this study.

The optical galaxy diameters D_{25} have been taken from the RC3 (de Vaucouleurs et al. 1991). Extraplanar dust detections are based on a study of our R–band images. This investigation

Table 4. Summary of eDIG detections and comparision with radio continuum observations

Galaxy	DIG morphology[a]	R [″], z [kpc][b]	SFR[$M_\odot$ yr^{-1}][c]	radio cont.[d]	log $L_{\rm FIR}$[e]
NGC 1963	disk: bright H II regions		0.05	no	43.143
	halo: diffuse extended emission, plumes	7W, 0.99			
IC 2531	disk: several H II regions		$\leq$0.13	no	
	halo: one filament	37W, ~ 2.0			
NGC 3044	disk: $\sim$ a dozen bright H II regions		0.71	yes/corr.	43.606
	halo: diffuse, plumes, loop	N/S layer: $1.1 - 1.8$			
NGC 4302	disk: absorption by dust, H II regions		0.13	yes/corr.	43.523
	halo: weak extraplanar layer + patches	$z \sim 0.8 - 0.9$			
NGC 4402	disk: H II regions embedded in DIG		0.07	yes	43.686
	halo: diffuse eDIG (localized)	16E, 2.2			
NGC 4634	disk: $\sim$ 10 bright H II regions		0.51	yes	43.383
	disk-halo interface: bright H II region	29W, 0.25			
	halo: diffuse, filaments	layer, $\sim$1.1			
	halo: Patch 1	15W, 1.4			
NGC 5170	disk: H II regions			yes	42.898
	halo: no eDIG	– – – –			
IC 4351	disk: H II regions			no	43.759
	halo: no eDIG	– – – –			
UGC 10288	disk: a few H II regions			yes	43.108
	halo: no eDIG (due to insuff. S/N)	– – – –			

[a] results from this investigation
[b] coplanar and extraplanar distances of eDIG from the galaxy center
[c] SFRs have been calculated according to Kennicutt (1998) using our derived Hα luminosities ($L_{\rm H\alpha}$)
[d] detections (yes), non-detections, or not yet observed (no), and correlations with Hα (corr.) from various radio continuum surveys (e.g., Hummel et al. 1991)
[e] FIR luminosities have been calculated from the FIR flux values given by Fullmer & Lonsdale (1989). No FIR luminosity for IC 2531 could be calculated since no FIR flux measurements were available.

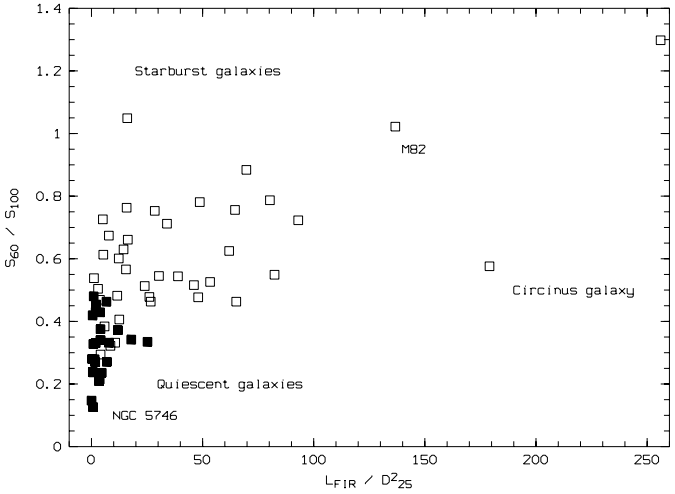

Fig. 11. Diagnostic diagram, showing the ratio of the flux densities at 60μm and 100μm expressed as S_{60}/S_{100} versus the ratio of the FIR luminosity ($L_{\rm FIR}$) divided by the optical diameter of the $25^{\rm th}$ mag/□″ isophote squared (D^2_{25})) in units of $10^{40}\,{\rm erg\,s^{-1}\,kpc^{-2}}$. The open squares denote positions occupied by starburst galaxies whereas the filled squares denote locations of normal or 'quiescent' galaxies. The starburst galaxies are essentially the sample studied by Lehnert & Heckman (1995). The galaxies indicated by the filled squares are galaxies currently investigated in the DIG context by various research groups (e.g., Pildis et al. 1994; Rand 1996; this study)

Table 5. DIG properties of the galaxies with gaseous halos

Galaxy	$N_{\rm H}[{\rm cm^{-2}}]$	$n_{\rm e}[{\rm cm^{-3}}]$	$M_{\rm DIG}[M_\odot]$
NGC 1963	1.05×10^{19}	0.0017	1.8×10^6
NGC 3044	4.85×10^{19}	0.0054	1.3×10^7
NGC 4302	6.05×10^{18}	0.0023	3.2×10^6
NGC 4402	1.19×10^{19}	0.0012	5.0×10^6
NGC 4634	4.36×10^{19}	0.0064	5.1×10^6

will be described separately in more detail (Rossa & Dettmar, in prep.).

In the following figure (Fig. 13) we have constructed a diagnostic DIG diagram (DDD) for our studied galaxies. Galaxies with extraplanar gas layers have been denoted by filled squares whereas galaxies with no extraplanar gas are indicated with open squares. The open triangle denotes the galaxy with extraplanar gas features (e.g., plumes), and where a weak extended layer has been detected. The plot is shown in a logarithmic scale.

Even with such a small sample it is evident that the galaxies with eDIG layers occupy certain regions in the DDD, whereas galaxies without eDIG halos do appear in different locations in this diagram. It is also clear that a larger sample of galaxies is necessary to make a quantitative approach in order to find

Table 6. Properties for diagnostic DIG diagrams

Galaxy	Type	T[a]	D [Mpc]	D_{25} [′]	S_{60}/S_{100}	$\mathrm{L_{FIR}}$ $[10^{43}\,\mathrm{erg\,s^{-1}}]$	$\mathrm{L/D^2_{25}}$ $[10^{40}\,\frac{\mathrm{erg}}{\mathrm{s\,kpc^2}}]$	extraplanar dust feat.
NGC 4634	Sc	6.0	19.1	2.57	0.3720	2.4247	11.892	yes
NGC 4402	Sb	3.0	22.0	3.89	0.3320	4.8664	7.853	yes
NGC 1963	Sc	5.5	17.7	2.82	0.4051	1.4494	6.954	yes
NGC 3044	SBb	5.0	17.2	4.90	0.4632	4.0546	6.746	
NGC 4302	Sc	5.0	18.8	5.50	0.2136	3.3496	3.703	yes
UGC 10288	Sc	5.3	27.3	4.79	0.2370	1.2882	0.890	
NGC 5170	Sc	5.0	20.0	8.32	0.2796	0.7940	0.339	no
IC 4351	Sb	3.0	35.5	5.75	0.1947	5.7577	1.633	no
IC 2531[b]	Sc	5.3	33.0	6.92	n	n	n	yes

[a] mean numerical index of stage along the Hubble sequence in RC2 system
[b] IC 2531 has not been detected with IRAS. Therefore no information concerning the FIR properties is available

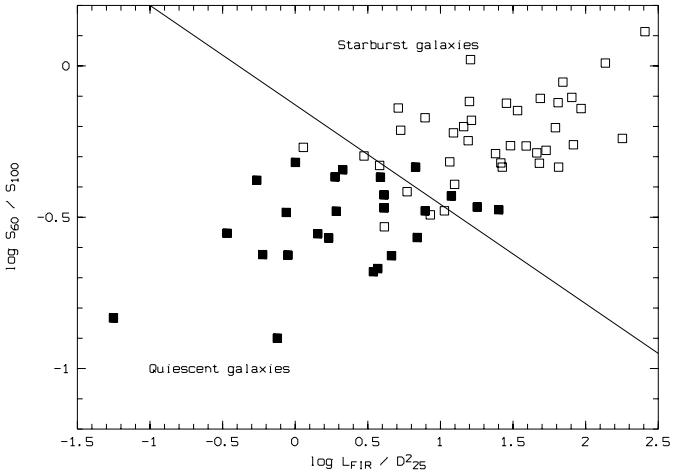

Fig. 12. Logarithmic diagram, showing the ratio of the flux densities at 60μm and 100μm expressed as S_{60}/S_{100} versus the ratio of the FIR luminosity (L_{FIR}) divided by the optical diameter of the 25^{th} mag/□″ isophote squared (D^2_{25}) in units of $10^{40}\,\mathrm{erg\,s^{-1}\,kpc^{-2}}$. The logarithmic plot shows the overlapping region in more detail. The open squares denotes areas occupied by starburst galaxies whereas the filled squares denote areas of normal or 'quiescent' galaxies. The solid line separates the two areas occupied by the various galaxy types, with an overlapping region, since some normal galaxies are also listed as starbursts in the literature and vice versa

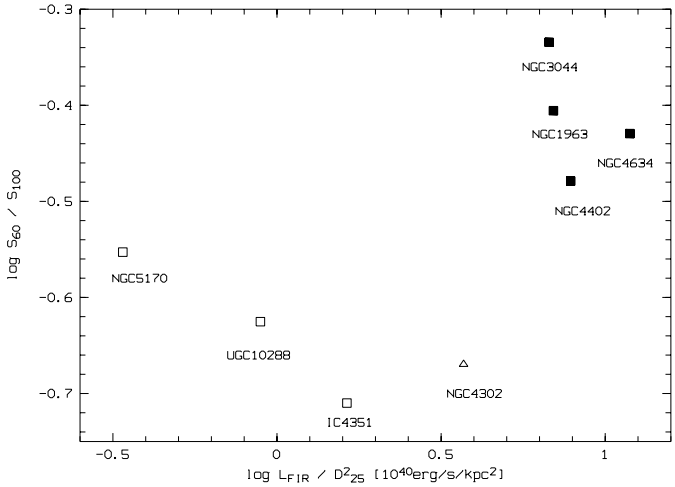

Fig. 13. Logarithmic diagram, showing the ratio of the flux densities at 60μm and 100μm expressed as S_{60}/S_{100} versus the ratio of the FIR luminosity (L_{FIR}) divided by the optical diameter of the 25^{th} mag/□″ isophote squared (D^2_{25}) in units of $10^{40}\,\mathrm{erg\,s^{-1}\,kpc^{-2}}$. The labels for the galaxies of our studied sample have been indicated. Filled squares denotes detections of extraplanar DIG layers, open squares indicate those with no detections, whereas the open triangle denotes the galaxy with eDIG features, but where only a weak layer has been detected

a limiting value of the ratio of $\frac{S_{60}}{S_{100}}/\frac{L_{\mathrm{FIR}}}{D^2_{25}}$ above that extended gaseous halos do exist.

Investigations to find this lower threshold are currently underway (Rossa & Dettmar, in prep.), where a much larger, distance limited and unbiased (in the sense of star formation activity) sample is covered.

5.2. Energetics of the outflow condition

In a study by Dahlem et al. (1995) it was concluded that the energy input of star formation regions into the ambient ISM, powered by SNe, is largest for galaxies with large and extended radio halos. In cases of low or non–detectable outflows (both Hα and radio continuum) such as NGC 4244 (Hummel et al. 1984), the faint end of the energy input rate has been reached. They use an important parameter as a measure of the disk–halo interaction (DHI), which is the threshold value of the energy injection into the ISM, which is given by $\frac{dE^{\mathrm{tot}}_{\mathrm{SN}}}{dt}/A_{\mathrm{SF}} = \nu_{\mathrm{SN}}\,E_{\mathrm{SN}}/2\pi\,r^2_{\mathrm{SF}}$. Here the total energy injection is the input from SNe ($\mathrm{E_{SN}} = 10^{51}\,\mathrm{erg\,s^{-1}}$). Depending on the derived SN rates (ν_{SN}), which might vary from 0.01 $\mathrm{yr^{-1}}$ to 0.05 $\mathrm{yr^{-1}}$ (van den Bergh 1991, and Dahlem et al. 1995, respectively), mean values of the total energy input of $1.5\times10^{-4}\,\mathrm{erg\,s^{-1}\,cm^{-2}}$ are derived.

However, gravitational interactions between the galaxies, such as in the case of NGC 4631 can lead to deviations from this trend that only high energy inputs powered by SNe lead to strong outflows. Therefore isolated galaxies should be considered as suitable candidates. The energy injection is of course highly

depending on the extend of the star formation activity area, where strong local SF activity is also in favor of strong outflows. This should be taken into account when selecting candidate galaxies with star formation driven outflows. Therefore a bias might result, if only FIR bright galaxies are selected. Galaxies with high local SF, despite a low FIR flux, would not be covered by this selection criterium. This is an important issue for future investigations.

6. Summary

We have presented the results of a small Hα survey aiming at the detection of extraplanar diffuse ionized gas (eDIG). 9 galaxies have been investigated. 4 of them show eDIG, whereby 2 others show only plumes, filaments, and in the case of NGC 4302 a faint eDIG layer is present. 3 galaxies do not show any signs of disk–halo interaction. The star formation rates have been derived for those edge–on galaxies, which showed bright diffuse emission. The morphology of the bright eDIG in NGC 4634 is similar to that of previously studied galaxies (e.g., NGC 891 and NGC 5775), although the emission is not as bright and far extended as in NGC 891. Furthermore a difference in comparison to NGC 891 is that the eDIG layer in NGC 4634 is symmetrically and homogeneously distributed, unlike the asymmetry which is observed in NGC 891.

The extraplanar filaments in NGC 4634 may be compared with the theoretical models such as the 'chimney' scenario by Norman & Ikeuchi, where the individual filaments (seen also in several other edge–on galaxies) may represent these very *chimneys*. However, this could probably only be investigated with high angular resolution studies, such as HST WFPC 2 observations. We have presented new evidence for disk–halo interaction in late–type galaxies (Sb–Sc). The fraction of DIG in the halo has been derived, and show that a significant mass of the gas is present in galaxy halos. It has become clear that eDIG is not observed in all late–type galaxies, and we argue that the DHI seems not to be a general case for all normal spirals. eDIG seems to be correlated with the star formation activity in the underlying disk, which is evidenced by the presence of star forming regions (e.g., H II regions) below the filaments. As a consequence, the galaxies with low SF activity show no or almost no gas outflows at the detection limit, which is given by the instrumentation. It also reflects the cosmic evolution of spiral galaxies with the episodes of star formation. The DIG mass has been derived for galaxies with extended DIG. These masses represent lower limits, since no correction for internal extinction has been applied.

Acknowledgements. The authors would like to thank Deutsches Zentrum für Luft– und Raumfahrt (DLR) for financial support of this research project through grant 50 0R 9707. It is a pleasure to thank Dr. D. Bomans for his helpful comments on the manuscript. We would like to thank the anonymous referee for useful suggestions, which helped to improve the presentation of the paper. This research has made extensive use of the NASA/IPAC Extragalactic Database (NED) which is operated by the Jet Propulsion Laboratory, California Institute of Technology, under contract with the National Aeronautics and Space Administration.

References

Barbon R., Cappellaro E., Turatto M., 1989, A&AS 81, 421
Binggeli B., Sandage A., Tammann G.A., 1985, AJ 90, 1681
Bregman J.N., Pildis R.A., 1994, ApJ 420, 570
Chevalier R.A., Clegg A.W., 1985, Nat 317, 44
Dahlem M., 1997, PASP 109, 1298
Dahlem M., Dettmar R.-J., Hummel E., 1994, A&A 290, 384
Dahlem M., Lisenfeld U., Golla G., 1995, ApJ 444, 119
Dahlem M., Weaver K.A., Heckman T.M., 1998, ApJS 118, 401
Dettmar R.-J., 1990, A&A 232, L15
Dettmar R.-J., 1992, Fund. Cosm. Phys. 15, 148
Dettmar R.-J., 1993, Rev. Mod. Astron. 6, 33
Dettmar R.-J., 1995, in: A. Ferrara et al. (eds.), The Physics of the Interstellar Medium and Intergalactic Medium, ASP Conf. Series No. 80, p. 398
Dettmar R.-J., Schulz H., 1992, A&A 254, L25
de Vaucouleurs G., de Vaucouleurs A., Corwin H.G. Jr., et al., 1991, Third Reference Catalogue of Bright Galaxies (RC 3), Springer Verlag
Domgörgen H., Mathis J.S., 1994, ApJ 428, 647
Domgörgen H., Dettmar R.-J., 1997, A&A 322, 391
Dove J.B., Shull J.M., 1994, ApJ 430, 222
Fabbiano G., Heckman T.M., Keel W.C., 1990, ApJ 355, 442
Ferguson A.M.N., Wyse R.F.G., Gallagher J.S. III, Hunter D.A., 1996, AJ 112, 2567
Fullmer L., Lonsdale C., 1989, Cataloged Galaxies and Quasars observed in the IRAS Survey, Jet Propulsion Laboratory
Golla G., Dettmar R.-J., Domgörgen H., 1996, A&A 313, 439
Heckman T.M., Armus L., Miley G.K., 1990, ApJS 74, 833
Helou G., Hoffman L.G., Salpeter E.E., 1984, ApJS 55, 433
Hoopes C.G., Walterbos R.A.M., Greenawalt B.E., 1996, AJ 112, 1429
Hoopes C.G., Walterbos R.A.M., Rand R.J., 1999, ApJ 522, 669
Howk J.C., Savage B.D., 1997, AJ 114, 2463
Howk J.C., Savage B.D., 1999, AJ 117, 2077
Hoyle F., Ellis G.R.A., 1963, Austr. J. Phys. 16, 1
Hummel E., van der Hulst J.M., 1989, A&AS 81, 51
Hummel E., Sancisi R., Ekers R.D., 1984, A&A 133, 1
Hummel E., Beck R., Dettmar R.-J., 1991, A&AS 87, 309
Just A., Fuchs B., Wielen R., 1996, A&A 309, 715
Kenney J.D.P., Koopmann R.A., 1999, AJ 117, 181
Kennicutt R.C. Jr., 1998, ApJ 498, 541
Kennicutt R.C. Jr., 1998b, Ann. Rev. of Astron. and Astroph. Vol. 36, p. 189
Kennicutt R.C. Jr., Kent S.M., 1983, AJ 88, 1094
Keppel J.W., Dettmar R.-J., Gallagher J.S. III, Roberts M.S., 1991, ApJ 374, 507
Lauberts A. 1982, The ESO/Uppsala Survey of the ESO (B) Atlas, European Southern Observatory
Lee S.-W., Irwin J.A., 1997, ApJ 490, 247
Lehnert M.D., Heckman T. M., 1995, ApJS 97, 89
Madau P., Pozzetti L., Dickinson M., 1998, ApJ 498, 106
Martin C.L., 1997, ApJ 491, 561
Mathis J.S., 1986, ApJ 301, 423
Miller W.W., Cox D.P., 1993, ApJ 417, 579
Niklas S., Klein U., Wielebinski R., 1995, A&A 293, 56
Nilson P. 1973, Uppsala General Catalogue of Galaxies, Nova Acta Regiae Societatis Scientiarum Upsaliensis, Ser. V, A, Vol. 1.
Norman C.A., Ikeuchi S., 1989, ApJ 345, 372
Oosterloo T., Shostak S., 1993, A&AS 99, 379
Osterbrock D.E. 1989, Astrophysics of Gaseous Nebulae and Active Galactic Nuclei, University Science Press

Pildis R.A., Bregman J.N., Schombert J.M., 1994, ApJ 427, 160
Quintana H., Ramírez A., 1995, ApJS 96, 343
Rand R.J., 1996, ApJ 462, 712
Rand R.J., 1997, ApJ 474, 129
Rand R.J., 1998, ApJ 501, 137
Rand R.J., Kulkarni S.R., Hester J.J., 1990, ApJ 352, L1
Rand R.J., Kulkarni S.R., Hester J.J., 1992, ApJ 396, 97
Reynolds R.J., 1984, ApJ 282, 193
Reynolds R.J., 1990, in: S. Bowyer and C. Leinert, (eds.), IAU Symp. No. 139, Galactic and Extragalactic Background Radiation, Kluwer, p. 157
Rush B., Malkan M.A., Spinoglio L., 1993, ApJS 89, 1
Salpeter E.E., 1955, ApJ 121, 161
Schroeder A., Visvanathan N., 1996, A&AS 118, 441
Shapiro P.R., Field G.B., 1976, ApJ 205, 762
Slavin J.D., Shull J.M., Begelman M.C., 1993, ApJ 407, 83
Soifer B.T., Sanders D.B., Madore B.F., et al., 1987, ApJ 320, 238
Teerikorpi P., Bottinelli L., Gouguenheim L., Paturel G., 1992, A&A 260, 17
Tüllmann R., Dettmar R.-J., 2000, submitted to A&A
Tully R.B., 1988, Nearby Galaxies Catalog, University of Cambridge Press
van den Bergh S., 1991, Phys. Rep. 204(6), 385